# Earth's magnetic field is (probably) not reversing

**Maxwell Brown**[a,b,1], **Monika Korte**[b], **Richard Holme**[c,d], **Ingo Wardinski**[b,e], **and Sydney Gunnarson**[a]

[a]Institute of Earth Sciences, University of Iceland, Sturlugata 7, 101 Reykjavík, Iceland; [b]GFZ German Research Centre for Geosciences, Telegrafenberg, 14473, Potsdam, Germany; [c]School of Environmental Sciences, University of Liverpool, Liverpool L69 3GP, United Kingdom; [d]Max Planck Institute for Solar System Research, Justus-von-Liebig-Weg 3 37077 Göttingen, Germany; [e]Laboratoire de Planétologie et de Géodynamique, Université de Nantes, UMR 6112 CNRS, F-44322 Nantes Cedex 3, France

This manuscript was compiled on March 9, 2018

**The geomagnetic field has been decaying at a rate of ∼5% per century from at least 1840, with indirect observations suggesting a decay since 1600 or even earlier. This has led to the assertion that the geomagnetic field may be undergoing a reversal or an excursion. We have derived a new model of the geomagnetic field spanning 30-50 ka, constructed to study the behavior of the two most recent excursions: the Laschamp and Mono Lake, centered at 41 ka and 34 ka, respectively. Here we show that neither excursion demonstrates field evolution similar to current changes in the geomagnetic field. At earlier times, centered at 49 ka and 46 ka, the field is comparable to today's field, with an intensity structure similar to today's South Atlantic Anomaly (SAA); however, neither of these SAA-like fields develop into an excursion or reversal. This suggests that the current weakened field will also recover without an extreme event such as an excursion or reversal. The SAA-like field structure at 46 ka appears to be coeval with published increases in geomagnetically modulated beryllium and chlorine nuclide production, despite the global dipole field not weakening significantly in our new model during this time. This agreement suggests a greater complexity in the relationship between cosmogenic nuclide production and the geomagnetic field than is commonly assumed.**

Geomagnetism | Paleomagnetism | Reversals | Excursions | Laschamp | South Atlantic Anomaly

Reversals and excursions have occurred numerous times in Earth history (1–4) and the recent behavior of the geomagnetic field has led to a discussion of whether we are in the early stages of a reversal or excursion (5–9). Since direct observations of the strength of the geomagnetic field began in 1840 (10, 11), it has decreased by ∼5% per century (12). This decay has been coupled to the growth and westward movement of a pronounced regional intensity low from southern Africa to South America, the so-called South Atlantic Anomaly (SAA) (see the panel for the 2015 field in Fig. 1). Indirect measurements of intensity obtained from fired archeological artefacts, volcanic rocks and sediments suggest that the current fall in intensity may have begun prior to 1840 (9, 13) and perhaps as early as 2000 years ago (14). It has been suggested that the SAA may continue to grow and initiate a reversal or excursion (8). Furthermore, conditions at the core-mantle boundary (CMB) related to long-lived structures such as the large low seismic shear wave velocity province (LLSVP) below southern Africa (15) may be responsible for the occurrence of geomagnetic field structures such as the SAA (16). Given the longevity of the African LLSVP, SAA-like structures have been suggested to be a recurrent feature of the geomagnetic field and a trigger for reversals/excursions (16, 17).

Although methods to forecast the geomagnetic field are in development (18, 19), they can not yet predict the field on long time scales. An alternative approach is to investigate the behavior of past reversals and excursions and infer whether the field structures we see today resemble those approaching reversals and excursions. As we go back in time the amount of data describing the temporal and spatial evolution of the geomagnetic field decreases, therefore, we concentrate our analysis on the two most recent excursions, the Laschamp at ∼41 ka (20, 21) and the Mono Lake at ∼34 ka. In this study we present the first temporally continuous global spherical harmonic model covering both the Laschamp and Mono Lake excursions and compare the geomagnetic field prior and during these excursions with today's geomagnetic field.

## 1. Results

In Fig. 1 we show maps of (1) the current field, (2) two snapshots of the field in a similar configuration to today (48.5 ka and 46.3 ka), and (3) two periods immediately following (2) that are dominated by the dipole, but do not have field structures similar to today (47.25 ka and 43.8 ka). These maps can be compared with snapshots of the field for the center of each excursion (Fig. 2), defined as local global minima in dipole moment (∼41 ka for the Laschamp excursion and ∼34 ka for the Mono Lake excursion) (Fig. 3). Further insights into the field structure are provided by an energy spectrum derived from the mean square field (23, 24) (see Materials and Methods). We determined spectra at two depths: the CMB, reflecting the physical origin of the field, and the surface, reflecting what is observed (movies of the spectra are provided

### Significance Statement

Earth's magnetic field is generated in Earth's convecting liquid iron outer core and protects Earth's surface from harmful solar radiation. The field has varied on different timescales throughout geological history and these variations reflect changes deep within the Earth. Two of the field's most extreme variations are reversals and excursions. During such events, the strength of the field decreases and the magnetic poles rapidly flip polarity, with reversals characterized by the pole retaining an opposite polarity, while excursions are marked by a return to the original polarity. Field strength over the past centuries has also been decreasing strongly; however, through analyzing previous excursions we infer that Earth's magnetic field is not in an early stage of a reversal or excursion.

MB initiated the project and with SG compiled and analyzed the paleomagnetic data. MK constructed the geomagnetic field model. RH noted the resemblance of the field prior to the Laschamp excursion to the current field, recognized the link between cosmogenic nuclide production and geomagnetic field structures at 46 ka and proposed the two base states idea. All authors interpreted the model output and contributed to writing the manuscript

The authors declare that they have no conflicts of interest.

[1]To whom correspondence should be addressed. E-mail: maxwell@hi.is

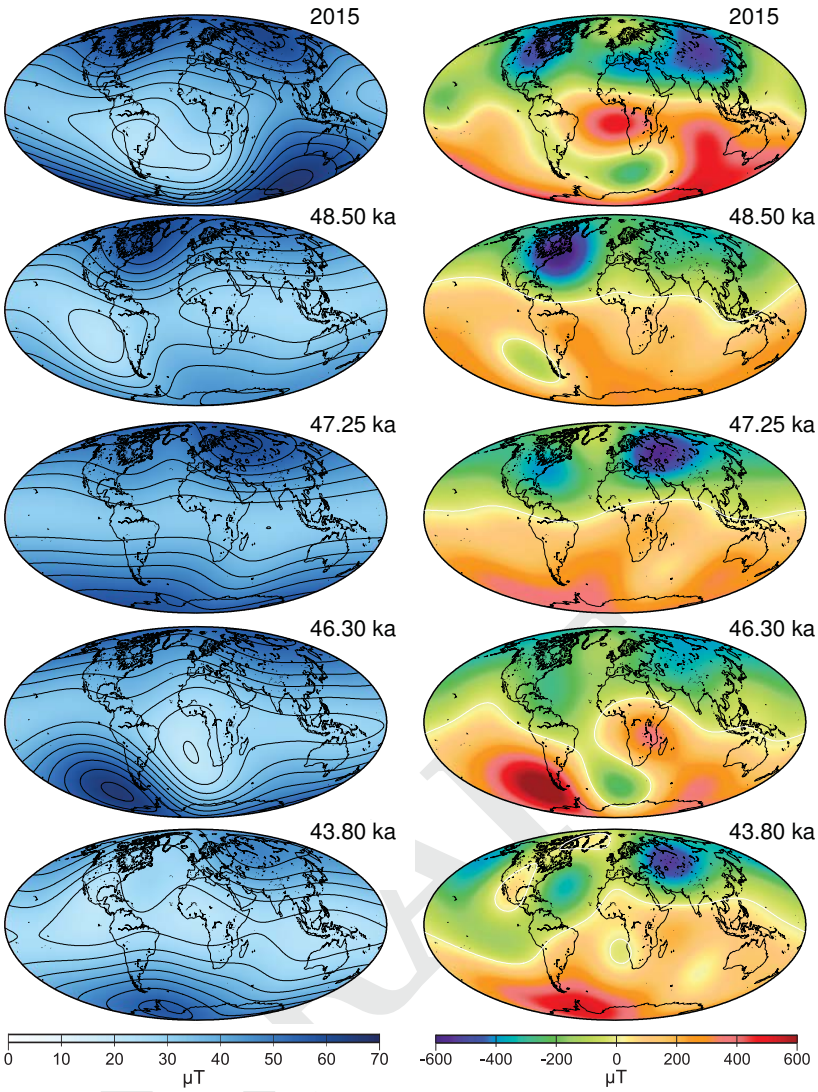


**Fig. 1.** Intensity at Earth's surface (left) and radial field ($Br$) at the CMB (right) for today's field (2015 from IGRF-12 (22)), examples of two SAA-like times (the 49 ka SAA at 48.5 ka and the 46 ka SAA at 46.3 ka) and two times that are dipole dominated at Earth's surface (47.25 ka and 43.8 ka). The field is truncated at spherical harmonic degree five.

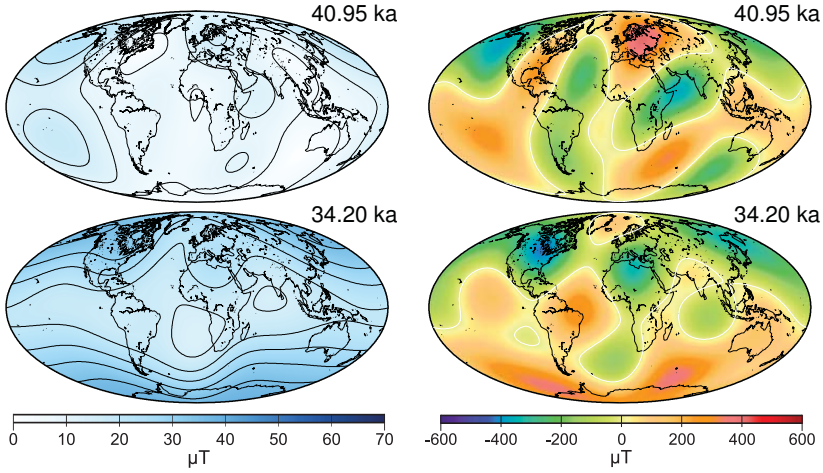


**Fig. 2.** Intensity at Earth's surface (left) and radial field ($Br$) at the CMB (right). Top: mid-point of the Laschamp excursion; bottom: mid-point of the Mono Lake excursion. The field is truncated at spherical harmonic degree five.

in Supporting Information). In Fig. 4 we summarize spectra for some of the snapshots in Fig. 1 and Fig. 2.

The two excursions display complex field structures that, unlike the current field, are either not dominated by the dipole field (as during the Laschamp excursion; Fig. 4c) or have a weaker dipole contribution than today (as during the Mono Lake excursion; Fig. 4d). However, the fields at 48.5 ka and 46.3 ka are highly reminiscent of the historical and recent field, as seen in the global models *gufm1* (10) and IGRF-12 (22) (Fig. 1). We refer to field structures similar to the current field with a minimum in intensity occurring across southern Africa, the south Atlantic or South America as SAA-like. The 48.5 ka and 46.3 ka snapshots belong to two epochs (50 ka to 47.8 ka and 47.2 to 45 ka) where SAA-like field structures are dominant. For simplicity we refer to these epochs as 49 ka and 46 ka, respectively. Following both SAA-like epochs, the field does not transition into an excursion or a reversal, rather, it reestablishes itself and strongly dipolar field structures become visible at Earth's surface (e.g., at 47.25 ka and 43.8 ka; Fig. 1). Prior to the Mono Lake excursion no apparent SAA-like structures are visible at Earth's surface (see the time-varying movie in Supporting Information).

The spectra for the SAA-like structures at 49 ka and 46 ka are similar to the present day (Fig. 4a,b), with an approximately white spectrum (common energy to all degrees), but with greater energy in the dipole field, indicating that the largest component of the field is the axial dipole, both at the surface and the CMB. The global surface field morphology is strongly altered during the SAA-like epochs, with the intensity of the field falling locally, e.g., by up to 60% within the 46 ka SAA; however, the dipole component decreases by only 10-20% globally (Fig. 3) and at a similar rate to that seen in recent Holocene field models over the past 2000 years (14). Although associated with a small decrease in the global dipole moment, the SAA-like surface fields are linked to growth of reversed flux patches at the CMB in the southern hemisphere coupled to variability in the non-dipole contributions to the field.

## 2. Discussion

**A. Comparing excursions and the present day field.** It has been suggested that the present day SAA may expand and deepen, leading to an excursion or reversal (8). Although the mechanisms that initiate these events could be different, the SAA-like intensity structures at 49 ka and 46 ka do not grow and spread across Earth's surface to form either excursions or reversals. Rather, the field remains dipole dominated during and after SAA-like epochs (Fig. 1 and 4). This leads us to infer that SAA-like structures are transitory and not diagnostic of an imminent excursion or reversal.

This finding does not imply that today's field will not continue its current decrease in intensity. This may persevere for some uncertain amount of time. The current global dipole moment is higher than during both the 49 ka and 46 ka SAA-like epochs (Fig. 3b) and could drop to at least these values. If the SAA continues to deepen, this will have the greatest consequences for the Americas. It has been noted that even a moderate decrease in dipole strength could have practical implications (25). For example, the current SAA has led to electrical failures on low Earth orbit satellites passing through the SAA (26) and with a continued decrease in field intensity, issues such as this will become more widespread.

**B. Initiation of excursions.** The generation of the excursions follows a different mechanism. For the Laschamp excursion, as for times prior to the 49 ka and 46 ka SAA-like events, the spectra are initially similar to the present day. However, from ∼43 ka onwards the axial dipole component weakens and the directional changes of the excursion are initiated slowly (Fig. 3). Two large intensity anomalies at the surface grow almost simultaneously (one over central America and one over SE Asia) and these are associated with the growth of reversed flux patches below these locations on the CMB. Through time the magnitude of the dipole begins to decay more rapidly and the energy spectrum at the CMB becomes white for all degrees at ∼42 ka (Fig. 4). This does not immediately yield large directional changes associated with the excursion (although some locations now have geomagnetic poles at equatorial latitudes), as even in this state the dipole energy at the surface exceeds the energy of non-dipole components. At just prior to 41 ka the non-dipole field begins to dominate at the surface as the fall in the axial dipole continues rapidly. Intensity anomalies at the surface grow and new spatially unconnected anomalies develop. Numerous reversed flux patches develop at the CMB, and immediately prior to 41 ka, reversed flux covers both poles (Fig. 2). At 41 ka the dipole reaches its minimum with a magnitude close to zero and then ceases to decay further (Fig. 3). Intensity is now low across the surface and fully reversed directions are observed at numerous locations; however, there is globally non-uniform directional variability with many locations showing only small directional excursions, as would be expected when the axial dipole reduces close to zero (Fig. 3), but does not reverse (27).

For the initiation of the Mono Lake excursion, the axial dipole begins to decay from a dipole dominated state around 36 ka. However, unlike the Laschamp excursion the decay in the axial dipole is only short lived with dipole energy remaining significantly above non-dipole energy at the surface (Fig. 3) and CMB (Fig. 4), with a minimum in the dipole moment occurring just prior to 34 ka. Multiple surface intensity anomalies appear at mid and low latitudes from 36 ka onwards, but they are short lived and erratic in their spatial evolution and do not resemble SAA-like field structures (see the movie in Supporting Information). Reversed flux patches start to develop after 35 ka, with reversed flux at mid- to high latitudes in both hemispheres appearing at ∼35 ka as the energy in the octupole term matches the energy of the dipole term. However, the Mono Lake excursion is not driven into a more substantial excursion, and by 33 ka the field regains its dominantly dipolar appearance at the surface, although increased energy in some of the higher order components post-33 ka creates greater spatial complexity in both intensity and $Br$ than for today's field.

**C. A mechanism for excursion and reversal generation.** A possible interpretation for excursions is that field contributions of all scales vary with time, but with a weaker base state (a weaker axial dipole), variations in the axial dipole are sufficient to produce an excursion (27). Excursions can therefore be considered a part of normal secular variation, but with a weaker axial dipole contribution and a greater chance of producing a zero or reversed dipole field. We argue that the field has two possible mean states, one in which the

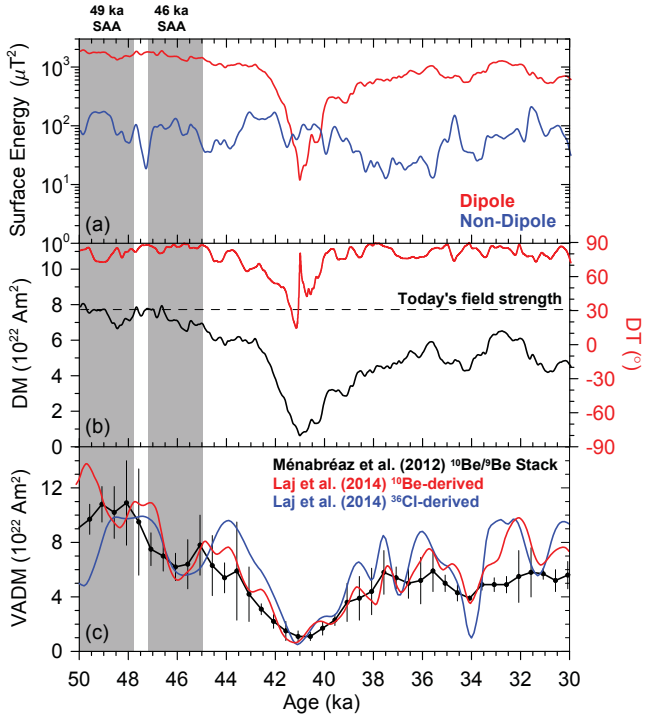


**Fig. 3.** Model time series between 30 ka and 50 ka. (a) Energy at Earth's surface (see Materials and Methods). (b) Dipole moment (DM) and dipole tilt (DT) (see Materials and Methods). (c) Virtual axial dipole moment (VADM) as a measure of geomagnetic field strength derived from cosmogenic nuclide records (data from original publications (28, 29)). The ice core $^{10}$Be- and $^{36}$Cl-derived dipole records were filtered at a frequency of 1/800 years to remove the influence of non-geomagnetically modulated cosmogenic nuclide production (28). Shaded areas are the times of the SAA-like fields around 49 ka and 46 ka.

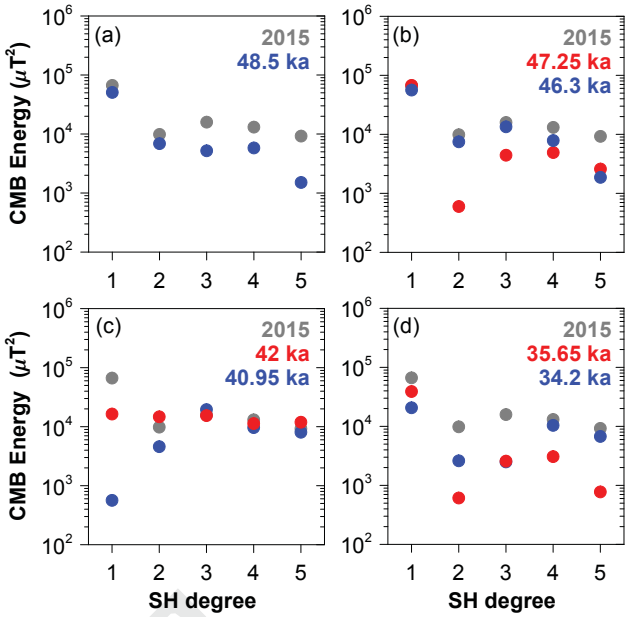


**Fig. 4.** Mean square field energy spectrum variations through spherical harmonic (SH) degrees 1 to 5 (see Materials and Methods). SH degree 1 is the dipole term. Red symbols are times preceding the 46 ka SAA epoch (b), the Laschamp excursion (c), and the Mono Lake excursion (d). Blue symbols are for times during the 49 ka and 46 ka SAA epochs, and at the mid-points of the two excursions. Grey symbols are for the 2015 IGRF-12 (22) field as a reference for today's field spectrum.

axial dipole is dominant at the CMB, which is broadly stable, and one in which the axial dipole matches the higher degrees, when fluctuations in the axial dipole can produce an excursion. The question remains, are random fluctuations sufficient for a full reversal? To answer this question, a reexamination of the most recent reversal, the Matuyama-Brunhes, building on previous modeling (30), but with an expanded data set, will be necessary.

We infer that for excursions to occur, a weakening of the field across much of the globe spreading from multiple sources is required, and not just localized weakening expanding from an SAA-like feature. They also require the growth of reversed flux patches in both hemispheres, with reversed flux transiting the poles. However, the amount and duration of reversed flux across the poles differs for the Laschamp and Mono Lake excursions. Reversed flux occurs simultaneously across both poles during the Laschamp (Fig. 2) and is present for ~2 ka, whereas across the Mono Lake, reversed flux is located primarily over the North Pole (Fig. 2) for only a few hundred years (see movie in Supporting Information).

Although today's dipole is weakening, it is still substantially stronger than the higher degree components of the field and exceeds the dipole moment from our model through the majority of 40-50 ka. Today's secular variation is instead comparable to the SAA-like states at 49 ka and 46 ka, which did not lead to an excursion. Similar arguments apply to the Mono Lake excursion; although it does not reach the magnitude and extent of the Laschamp excursion, it still starts from a more geographically-spread weak state than from a single SAA-like feature.

**D. Relationship between SAA-like structures and cosmogenic nuclide production.** The above inferences depend on the robustness of our model; however, there is evidence from a complementary source: variations in cosmogenic nuclide production. Peaks in nuclide production ($^{10}$Be and $^{36}$Cl) coincide with the intensity lows of the Laschamp (29, 31) and Mono Lake (31, 32) excursions (Fig. 3c). However, there are also peaks in production that do not match known excursions. One production peak of particular note occurs at 46 ka and is coeval with one of our SAA-like structures, supporting our observation of a weakened field at this time. This peak is evident as a low in the 1/800 year filtered $^{10}$Be- and $^{36}$Cl-derived dipole variations obtained from Greenland ice core records (7, 28) and is hinted at in the stacks of sediment $^{10}$Be/$^{9}$Be records from the Portuguese margin and west equatorial Pacific (29) (Fig. 3c). There are two other times when there are decreases in both the $^{10}$Be- and $^{36}$Cl-derived dipole data. The low at ~31 ka is approximately coeval with a decrease in dipole moment in our model. The low at ~37 ka does not appear to be correlated with any field behavior in our model; however, this low appears negligible in the same records filtered at 1/3000 years (31). The origin of the anti-correlation of the $^{10}$Be- and $^{36}$Cl-derived dipole ice core records between 49-50 ka is currently unknown (31) and we do not consider cosmogenic nuclide data prior to 48 ka in our analysis.

Cosmogenic nuclide records reflect globally averaged production through post-production atmospheric mixing processes (33). Numerous factors can influence cosmogenic nuclide pro-

duction and concentration (31). On time scales longer than hundreds of years, production results primarily from variations in the geomagnetic field, although possible millennial scale solar activity and climate influences may complicate estimates of dipole change (31). It is commonly assumed that production is related to changes in the dipole component of the field. This is based on the altitude of modulation of cosmic rays and the rapid fall-off of non-dipole components with distance from the CMB (31). However, we observe only a minor reduction in dipole moment at 46 ka in our model (Fig. 3) and suggest instead that localized areas of weak intensity, such as SAA-like structures, might additionally allow cosmogenic nuclides to penetrate the geomagnetic field. We do not claim that the apparently coveal timing of one our SAA-like structures with a period of increased cosmogenic nuclide production unequivocally links the two events; however, this observation would be worth pursuing by researchers in the future. This conjecture could be tested by incorporating the geomagnetic model presented here into models of cosmogenic nuclide production for this time.

## Materials and Methods

The data used for modeling can be found in (34). Our analysis derives from a new model of the time-dependent geomagnetic field spanning 30 to 50 ka. The model was constructed from the largest compilation of sediment and volcanic paleomagnetic data for this period to date (see SI Appendix), exceeding the amount of data used in the only previous attempt to model the Laschamp excursion (35). An inverse model was constructed using a spherical harmonic decomposition of the scalar potential for the field $B = \nabla\Phi$, with each coefficient expanded in time on a basis of cubic B-splines, following methods used for the historical (10) and Holocene field (14, 36, 37). The spatial series was expanded to spherical harmonic degree and order 10, and spline knot points were placed every 50 years. This allowed for more complexity in the model than we expected to recover from the available data. Regularizations in space and time were invoked to trade-off a reasonable fit to the data against smooth models, i.e. those requiring the least amount of structure to describe the data. We used physically motivated regularization constraints: the Ohmic dissipation norm in space and the second derivative of the radial field component in time. The model coefficients were determined from the data under the regularization constraints using a least-squares approach. Declination, inclination and intensity data are non-linearly related to the model coefficients, therefore, the problem was linearized and the solution found iteratively. The model was based on 35 iteration steps to ensure convergence (38). This description allows us to plot maps both of the field observed at Earth's surface and the radial magnetic field ($Br$) at the core mantle boundary (CMB), the region of the field's origin. (Movies of $Br$ at the CMB and total field strength at Earth's surface are provided in Supporting Information.)

The data uncertainties are insufficiently defined to be used to constrain the appropriate smoothness of the model through a given fit to the data. Instead, following previous Holocene geomagnetic field modeling (38), the spatial damping parameter was chosen by comparing the main-field energy spectra at times before and after the Laschamp excursion with the present-day spectrum. This ensured that for degree $\geq 2$, the energy in each degree was not substantially higher than for the present-day field (38). With our chosen regularization constraint the spectrum falls off rapidly beyond spherical harmonic degrees four or five, suggesting that the data are insufficient for effective model resolution beyond these degrees. All model output in the figures have been truncated to degree five. To test whether our model is capable of resolving SAA-like field structures up to degree five, we truncated the IGRF-12 model for 2015 to different spherical harmonic degrees. The surface intensity anomaly is visible even at degree two, with radial field structures appearing at degrees four and five (see SI Appendix for further details on this test).

Given the inherent temporal smoothing of the paleomagnetic signal in sediment data (depending on sedimentation rate and other mechanism affecting remanence acquisition and/or sampling/measurement method), the secular variation energy will be lower than for models of the present-day geomagnetic field. We chose the strength of temporal regularization through a visual comparison of data and model predictions, such that the model on average did not show more temporal variability than reasonably required by the data (see SI Appendix, Fig. S4-S6 and Fig. S10-S12).

The parameters used to describe magnetic field evolution are as follows. The mean square field (23, 24) is given by

$$\int B(r)^2 d\Omega = \sum_{l}^{l_{max}} (l+1) \left(\frac{a}{r}\right)^{2l+4} \sum_{m=0}^{l} [(g_l^m)^2 + (h_l^m)^2], \quad [1]$$

where $g_l^m$ and $h_l^m$ are the Schmidt-normalised Gauss coefficients of spherical harmonic degree $l$ and order $m$, $a$ is the radius to be investigated, and $r$ is the mean radius of the solid Earth. In Fig. 4 the contributions to this quantity are separated by spherical harmonic degree, and the energy at each degree, $l$, plotted against that degree. The energy of the dipole ($R_d$) and non-dipole ($R_{nd}$) field plotted in Fig. 3 are limited to degree and order 5 and are given by

$$R_d = 2 \left(\frac{a}{r}\right)^6 (g_1^0)^2 + (g_1^1)^2 + (h_1^1)^2 \quad [2]$$

and

$$R_{nd} = \sum_{l=2}^{5} \left[ (l+1) \left(\frac{a}{r}\right)^{2l+4} \sum_{m=0}^{l} \left( (g_l^m)^2 + (h_l^m)^2 \right) \right], \quad [3]$$

The dipole moment (DM) at Earth's surface plotted in Fig. 3 is given by

$$DM = \frac{4\pi}{\mu_0} a^3 \sqrt{(g_1^0)^2 + (g_1^1)^2 + (h_1^1)^2}, \quad [4]$$

where $\mu = 4\pi \cdot 10^{-7}$ Vs/Am, the permeability of free space. The latitude of the dipole axis (DT) plotted in Fig. 3 is given by

$$DT = tan^{-1} \left( \frac{g_1^0}{\sqrt{(g_1^1)^2 + (h_1^1)^2}} \right). \quad [5]$$

**ACKNOWLEDGMENTS.** Funding was provided by the Deutsche Forschungsgemeinshcaft (DFG) through SPP PlanetMag 1488 project BR4697/1. RH was supported by a Gauss Professorship from the Akademie der Wissenschaften zu Göttingen. IW was supported by the French ANR project ANR-13-BS05-0012 (Marmite). Sanja Panovska and Lisa Tauxe are thanked for providing their data compilations. The authors of individual studies who provided data are thanked. MB acknowledges discussions with Norbert Nowaczyk and Roman Leonhardt.

### References.

1. Cande SC, Kent DV (1995) Revised calibration of the geomagnetic timescale for the late Cretaceous and Cenozoic. *J. Geophys. Res.* 100:6093–6095.
2. Laj C, Channell JET (2007) 5.10 - geomagnetic excursions in *Treatise on Geophysics*, ed. Schubert G. (Elsevier, Amsterdam), pp. 373–416.
3. Ogg J (2012) Chapter 5 - Geomagnetic Polarity Time Scale in *The Geologic Time Scale*, eds. Gradstein FM, Ogg JG, Schmitz MD, Ogg GM. (Elsevier, Boston), pp. 85 – 113.
4. Singer BS (2014) A Quaternary geomagnetic instability time scale. *Quat. Geochron.* 21:29–52.
5. Hulot G, Eymin C, Langlais B, Mandea M, Olson N (2002) Small-scale structure of the geodynamo inferred from Oersted and Magsat satellite data. *Nature* 416:620–623.
6. Constable C, Korte M (2006) Is Earth's magnetic field reversing? *Earth Planet. Sci. Lett.* 246:1–16.
7. Laj C, Kissel C (2015) An impending geomagnetic transition? Hints from the past. *Frontiers in Earth Science* 3(61).
8. Pavón-Carrasco FJ, De Santis A (2016) The South Atlantic Anomaly: the key for a possible geomagnetic reversal. *Frontiers in Earth Science* 4(40).
9. Poletti W, Biggin AJ, Trindade RI, Hartmann GA, Terra-Nova F (2018) Continuous millennial decrease of the earth's magnetic axial dipole. *Phys. Earth Planet. Inter.* 274:72–86.
10. Jackson A, Jonkers ART, Walker MR (2000) Four centuries of geomagnetic secular variation from historical records. *Phil. Trans. R. Soc. Lond. A* 358:957–990.
11. Jonkers ART, Jackson A, Murray A (2003) Four centuries of geomagnetic data from historical records. *Rev. Geophys.* 41(2):1006.
12. Gubbins D, Jones A, Finlay CC (2006) Fall in the Earth's field is erratic. *Science* 312:900–902.

13. Suttie N, Holme R, Hill MJ, Shaw J (2011) Consistent treatment of errors in archaeointensity implies rapid decay of the dipole prior to 1840. *Earth Planet. Sci. Lett.* 304:13–21.
14. Constable C, Korte M, Panovska S (2016) Persistent high paleosecular variation activity in southern hemisphere for at least 10 000 years. *Earth Planet. Sci. Lett.* 453:78–86.
15. Garnero EJ, McNamara AK (2008) Structure and dynamics of Earth's lower mantle. *Science* 320:626–628.
16. Tarduno JA, et al. (2015) Antiquity of the South Atlantic Anomaly and evidence for top-down control on the geodynamo. *Nature Communications* 6:7865.
17. Gubbins D (1987) Mechanism for geomagnetic polarity reversals. *Nature* 326:167–169.
18. Fournier A, et al. (2010) An introduction to data assimilation and predictability in geomagnetism. *Space Science Reviews* 155:247–291.
19. Tangborn A, Kuang W (2018) Impact of archeomagnetic field model data on modern era geomagnetic forecasts. *Phys. Earth Planet. Inter.* 276:2–9.
20. Singer BS, et al. (2009) $^{40}$Ar/$^{39}$Ar, K-Ar and $^{230}$Th-$^{238}$U dating of the Laschamp excursion: A radioisotopic tie-point for ice core and climate chronologies. *Earth Planet. Sci. Lett.* 286:80–88.
21. Lascu I, Feinberg JM, Dorale JA, Cheng H, Edwards RL (2016) Age of the Laschamp excursion determined by U-Th dating of a speleothem geomagnetic record from North America. *Geology* 44(2):139–142.
22. Thébault E, et al. (2015) International Geomagnetic Reference Field: the 12th generation. *Earth, Planets and Space* 67(1):79.
23. Lowes FJ (1966) Mean-square values on sphere of spherical harmonic vector fields. *J. Geophys. Res.* 71(8):2179–2179.
24. Lowes FJ (1974) Spatial power spectrum of the main geomagnetic field, and extrapolation to the core. *Geophys. J. R. astr. Soc.* 36(3):717–730.
25. Olson P, Amit H (2006) Changes in earth's dipole. *Naturwissenschaften* 93:519–542.
26. Heirtzler JR, Allen JH, Wilkinson DC (2002) Ever-present South Atlantic Anomaly damages spacecraft. *Eos, Transactions American Geophysical Union* 83(15):165–169.
27. Brown MC, Korte M (2016) A simple model for geomagnetic field excursions and inferences for palaeomagnetic observations. *Physics of the Earth and Planetary Interiors* 254:1–11.
28. Laj C, Guillou H, Kissel C (2014) Dynamics of the earth magnetic field in the 10-75 kyr period comprising the Laschamp and Mono Lake excursions: New results from the French Chaîne des Puys in a global perspective. *Earth Planet. Sci. Lett.* 387:184–197.
29. Ménabréaz L, Bourlès DL, Thouveny N (2012) Amplitude and timing of the Laschamp geomagnetic dipole low from the global atmospheric $^{10}$Be overproduction: Contribution of authigenic $^{10}$Be/$^{9}$Be ratios in west equatorial Pacific sediments. *J. Geophys. Res.* 117(B11101).
30. Leonhardt R, Fabian K (2007) Paleomagnetic reconstruction of the global geomagnetic field evolution during the Matuyama/Brunhes transition: iterative Bayesian inversion and independent verification. *Earth Planet. Sci. Lett.* 253:172–195.
31. Muscheler R, Beer J, Kubik PW, Synal HA (2005) Geomagnetic field intensity during the last 60,000 years based on $^{10}$Be and $^{36}$Cl from the Summit ice cores and $^{14}$C. *Quat. Sci. Rev.* 24:1849–1860.
32. Wagner G, et al. (2000) Chlorine-36 evidence for the Mono Lake event in the Summit GRIP ice core. *Earth Planet. Sci. Lett.* 181:1–6.
33. Masarik J, Beer J (1999) Simulation of particle fluxes and cosmogenic nuclide production in the Earth's atmosphere. *J. Geophys. Res.* 104:12099–12111.
34. Brown MC, Korte M, Holme R, Wardinski W, Gunnarson S (2018) Compilation of palaeomagnetic data from sediments and volcanic rocks spanning 30,000 to 50,000 years ago used to create the temporally continuous global spherical harmonic geomagnetic field model LSMOD.1. V. 1. GFZ Data Services. http://doi.org/10.5880/GFZ.2.3.2018.002.
35. Leonhardt R, et al. (2009) Geomagnetic field evolution during the Laschamp excursion. *Earth Planet. Sci. Lett.* 278:87–95.
36. Korte M, Constable C, Donadini F, Holme R (2011) Reconstructing the Holocene geomagnetic field. *Earth Planet. Sci. Lett.* 312:497–505.
37. Constable C, Korte M (2015) Centennial- to millennial-scale geomagnetic field variations in *Treatise on Geophysics, Second Edition*. (Elsevier, Amsterdam, Netherlands).
38. Korte M, Donadini F, Constable CG (2009) Geomagnetic field for 0-3 ka: 2. a new series of time-varying global models. *Geochem. Geophys. Geosyst.* 10:Q06008.

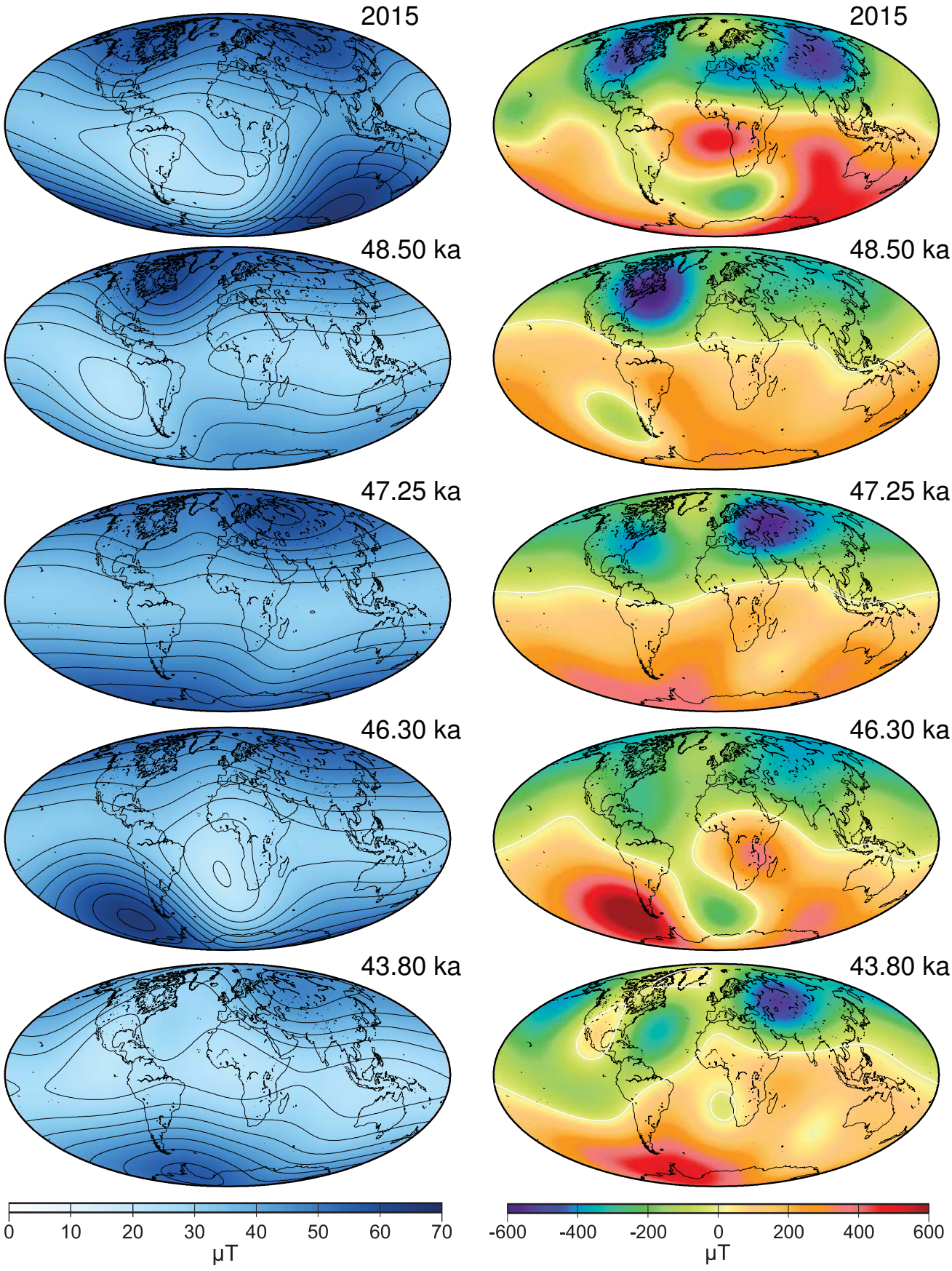
2015
2015
48.50 ka
48.50 ka
47.25 ka
47.25 ka
46.30 ka
46.30 ka
43.80 ka
43.80 ka
0
10
20
30
40
50
60
70
μT
-600
-400
-200
0
200
400
600
μT

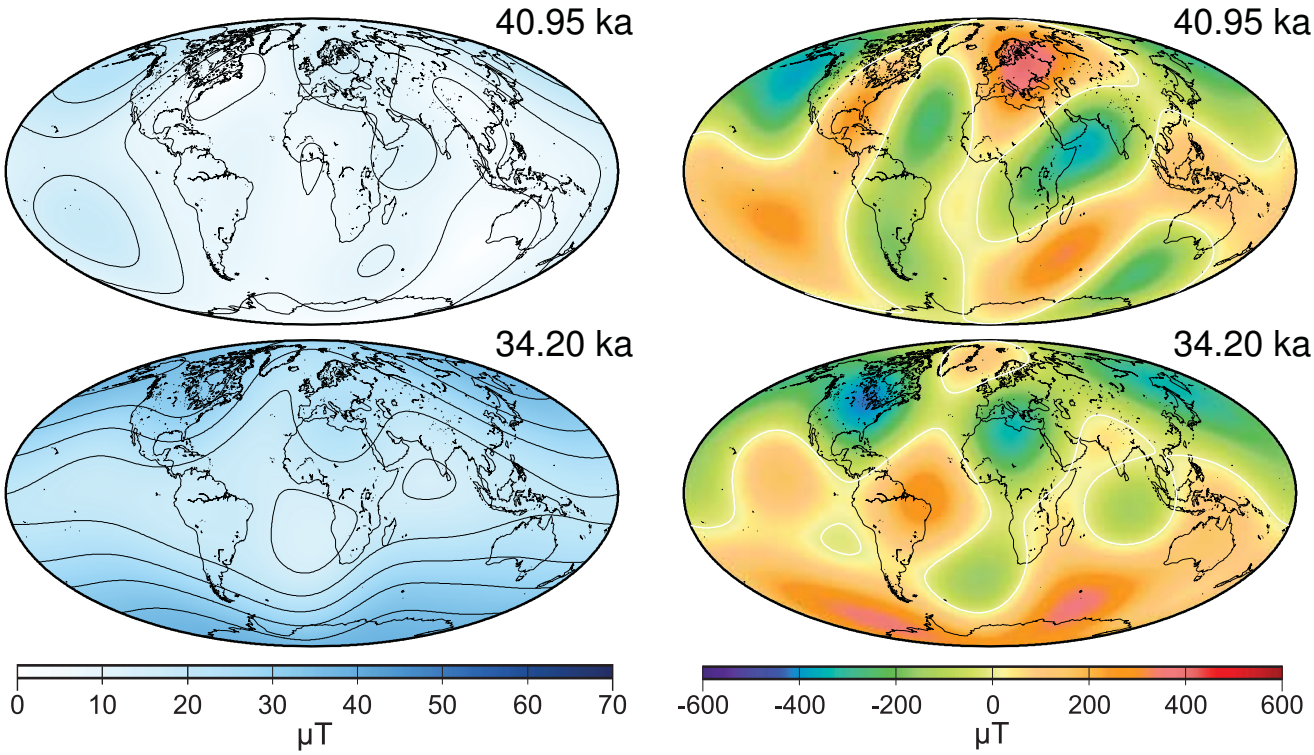
40.95 ka
40.95 ka
34.20 ka
34.20 ka
0
10
20
30
40
50
60
70
μT
-600
-400
-200
0
200
400
600
μT

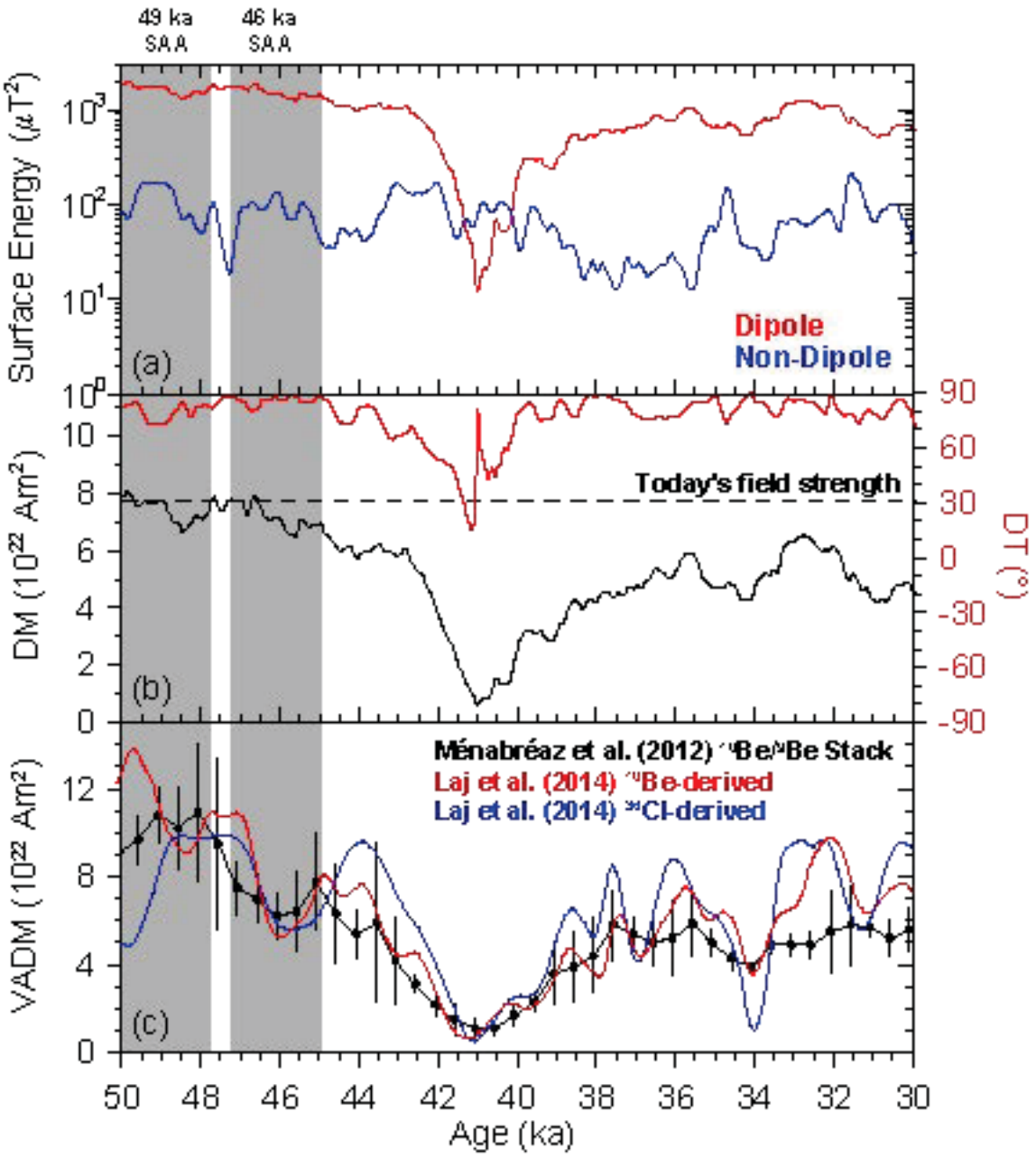
49 ka
SAA
46 ka
SAA
Surface Energy (μT²)
Dipole
Non-Dipole
(a)
DM (10²² Am²)
Today's field strength
DT (°)
(b)
VADM (10²² Am²)
Ménabréaz et al. (2012) ¹⁰Be/⁹Be Stack
Laj et al. (2014) ¹⁰Be-derived
Laj et al. (2014) ³⁶Cl-derived
(c)
Age (ka)

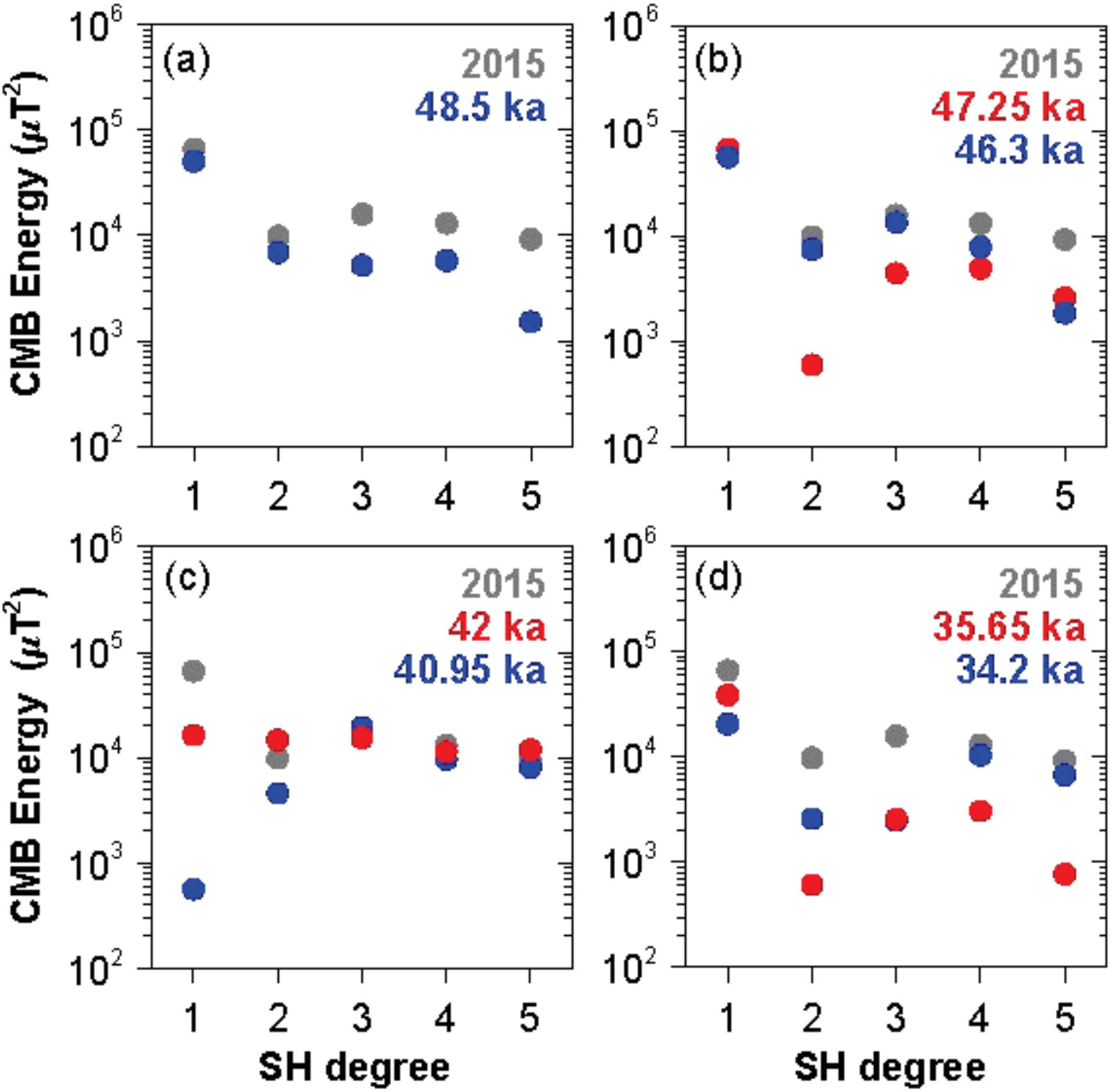
(a)
2015
48.5 ka
(b)
2015
47.25 ka
46.3 ka
(c)
2015
42 ka
40.95 ka
(d)
2015
35.65 ka
34.2 ka
CMB Energy (μT²)
SH degree
10⁶
10⁵
10⁴
10³
10²
1
2
3
4
5